PUBLICATION REFERENCE
Ntziachristos V "Going deeper than microscopy: the optical imaging frontier in biology"
Nature Methods 7(8); 603-614 (2010) doi:10.1038/nmeth.1483

Going deeper than microscopy: the optical imaging frontier in biology

Ntziachristos V

Optical microscopy has been a fundamental tool of biological discovery for more than three centuries, but its in vivo tissue imaging ability has been restricted by light scattering to superficial investigations, even when confocal or multiphoton methods are used. Recent advances in optical and optoacoustic (photoacoustic) imaging now allow imaging at depths and resolutions unprecedented for optical methods. These abilities are increasingly important to understand the dynamic interactions of cellular processes at different systems levels, a major challenge of postgenome biology. This Review discusses promising photonic methods that have the ability to visualize cellular and subcellular components in tissues across different penetration scales. The methods are classified into microscopic, mesoscopic and macroscopic approaches, according to the tissue depth at which they operate. Key characteristics associated with different imaging implementations are described and the potential of these technologies in biological applications is discussed.

For centuries, biological imaging was myopic; visualization stopped at about 10 µm of tissue depth. Detailed observation of tissue came with a death sentence for the tissue (fixation) so that it could be observed by histology. Naturally transparent organisms such as *Caenorhabditis elegans* or the early stage *Danio rerio* were exceptions, as were monolayers of cultured cells. Consequently, these became biology's workhorses in understanding longitudinal processes in development and disease.

The imaging limit of conventional microscopy can be derived from a physical parameter called the mean free path (MFP) of a photon. The MFP describes the average distance that a photon travels between two consecutive scattering events (Box 1 and Fig. 1). Scattering occurs in other types of electromagnetic radiation such as in X-ray or γ-ray spectral regions, but it is particularly strong in the ultraviolet (<450 nm), visible (450–650 nm) and near-infrared (650–1,000 nm) spectral regions owing to photon interaction with cellular structuresinteraction with cellular the near-infrared spectral region than in the visible and ultraviolet regions. The MFP is of the order of 100 µm in tissue, although it varies with tissue type; it is shorter in highly scattering tissues such as lung or muscle and longer in low-scattering tissues such as naturally semitransparent organisms. This means that the bulk of photons propagating through a 100-µm tissue slice will experience at least one scattering event, resulting in image blur. The traditional 10–20-µm thickness of tissue slices used for microscopy ensures that only a small fraction of photons are scattered, resulting in high image quality and diffraction-limited resolution.

Confocal and multiphoton microscopy have been developed to image specimens thicker than 10–20 µm, that is, at depths where photon scattering occurs[2–4]. These methods have revolutionized biological discovery by allowing the noninvasive study of life processes in unperturbed environments because high-resolution images can be formed at depths of several tenths to hundreds of micrometers. The penetration limit of these advanced forms of microscopy is governed by a second physical parameter, the transport mean free path (TMFP), which takes into account the MFP and the average angle by which photons are scattered in each scattering event. Multiple scattering events effectively randomize the photon propagation direction resulting in photon diffusion. In this case, the higher the scattering angle, the shorter the distance that it takes for photons to become diffusive. TMFP indicates the mean propagation distance that it takes for photons to, on average, lose relation to the propagation direction they had before entering tissue. In many animal and human tissues, TMFP is typically ten times larger than MFP, although it greatly depends on the tissue type and wavelength of operation (Box 1 and Table 1), and represents an upper limit of the penetration of microscopic techniques. Confocal or multiphoton microscopy, for example, operate at penetration depths that are smaller than 1 TMFP. Imaging beyond 1 TMPF with optical methods has been traditionally challenging. Biological imaging

Institute for Biological and Medical Imaging, Helmholtz Zentrum München und Technische Universität München, Munich, Germany. Correspondence should be addressed to V.N. (v.ntziachristos@tum.de).

Box 1: Photon Propagation in Tissues

The interaction of photons with different cellular structures results in elastic scattering. Scattering is a process of photon absorption and re-emission without loss of energy but possibly associated with a change in photon direction. For biological structures, the re-emission has a high probability to be in the forward direction for each scattering event. Despite this, the accumulation of multiple scattering events results in a gradual randomization of the propagation direction.

The mean free path (MFP) in tissue is defined as $1/\mu t$, in which μt is the transport coefficient, typically expressed as a sum of the tissue's absorption coefficient μa and the tissue's scattering coefficient μs, that is, $\mu t = \mu a + \mu s$. As $\mu s >> \mu a$ in most tissues, MFP can be simply written as

$$MFP = 1/\mu s.$$

When considering a photon undergoing several scattering events, the reduced scattering coefficient can be defined[50,94,95] to describe this multiple scattering process as $\mu s' = \mu s\ (1 - g)$, in which g is the anisotropy function defining the degree of forward scattering, expressed as a probability function of scattering in the forward direction described by a Henyey-Greenstein phase function with a coefficient, g. For photon scattering in tissue, g is typically 0.8–1. The transport mean free path (TMFP) can then be defined as

$$TMFP = 1/\mu s'$$

also assuming that scattering is dominant over absorption, that is, $\mu s' >> \mu a$, which generally holds for most tissues. Therefore, MFP = TMFP $(1 - g)$, an equation that describes the relation of the two parameters (Fig. 1). The higher the g, the more forward the scattering and the longer it takes for light to become diffuse, resulting in higher penetration distances with microscopic techniques. Table 1 summarizes μa, $\mu s'$ and TMFP values for different tissues, compiled as averages for the near-infrared spectral region (650–1,000 nm) from refs. [49,96–99].

The underlying photon propagation process can be understood if we consider that photons after $(1 - g)-1$ scattering events reach a random propagation compared to the direction of the incident beam. Therefore, although the propagation between 0 and 1 MFP is largely ballistic, as the travel distance increases to 1 TMFP, there is increasingly more scattering, eventually leading to photon diffusion.

Table 1 Optical properties of different tissues

Tissue type	**Absorption coefficient (cm−1)**	**Reduced scattering coefficient (cm−1)**	**TMFP (mm)**
Muscle	0.20	9	1.1
Brain	0.25	16	0.6
Breast	0.05	12	0.8
Lung	0.10	30	0.3

Data are compiled from previously published work (see **Box 1**).

beyond this limit has typically relied on non-optical approaches such as X-ray computed tomography (XCT), magnetic resonance imaging (MRI), ultrasound and positron emission tomography or single-photon emission tomography adapted to small-animal dimensions. However, the increasing need to study biological processes *in vivo* using methods more readily available to the biologist has driven the development of photonic methods that can be used to image well beyond the penetration limits of conventional microscopy. Here I review established and emerging photonic methods, focusing on methodologies that can perform *in vivo* molecular imaging, that is, *in vivo* imaging of optical reporters such as fluorescent probes, fluorescent proteins and other chromophoric agents and nanoparticles that can be used to label cellular and subcellular moieties and processes[5,6]. I classify the different methods in relation to their penetration depth measured in TMFP units as follows: microscopy, denoting depths smaller than 1 TMFP (typically <0.5–1 mm); macroscopy, denoting depths larger than 10 TMFP (typically >1 cm); and mesoscopy, indicating depths of 1–10 TMFP (typically 0.5 mm to 1 cm). Although other classifications are possible, for example, based on resolution or on the technology used, I selected the classification based on operation depth and described by MFP and TMFP because it allows for a direct comparison of tissue imaging photonic techniques against scattering, an important limiting factor. For each depth regime, I discuss relevant technologies, their performance characteristics and application areas.

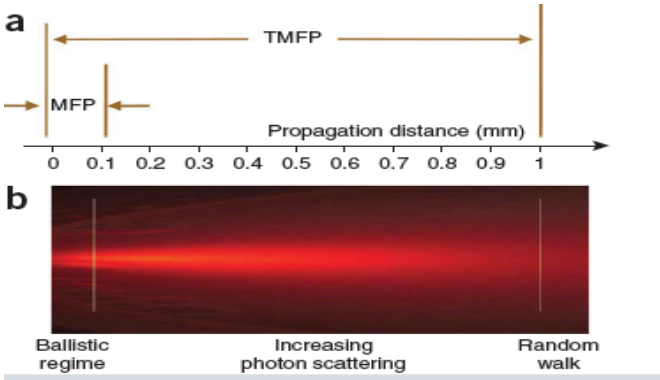

Figure 1 | Simplified metrics of photon propagation in tissue. (a,b) Schematic depiction of MFP and TMFP (a) and of photon propagation (b). The scale in physical dimensions is indicative of an average tissue with a reduced scattering coefficient of 10 cm−1. This scale will vary depending on the tissue and the wavelength used.

Deep-tissue microscopic imaging

Microscopy generates images at resolutions below those achieved by the naked eye. The performance of many advanced microscopy systems depends upon the ability of a lens to focus light on or in tissue. Photon scattering, which degrades this ability at increasing depth, fundamentally limits the penetration capacity of microscopic imaging.

Confocal and multiphoton microscopy. The most widely used technologies for *in vivo* microscopy of tissues are confocal and two- or multiphoton (2P/MP) microscopy[7,8]. In contrast to conventional microscopy that requires thin tissue sections, confocal and 2P/MP microscopy can achieve up to diffraction-limited resolution when imaging virtual tissue sections in intact tissue volumes, which is an aspect of these methods referred to as 'tissue sectioning' or 'optical sectioning'. In particular, laser scanning confocal microscopy scans a focused laser beam inside the specimen and uses a pinhole to reject photons that arrive to the detector from out-of-focus areas; these have been typically scattered multiple times and contribute to image blurring. Although the pinhole rejects a large part of the photons, sufficient signal from the focal point can be detected using high-intensity light sources and sensitive detectors. Two-dimensional 'tissue sections' are formed by scanning the focused beam over a plane in the sample imaged and piecing together information from each individual focal area. As information is collected only from the laser focal spot at each time point, single element detectors such as photomultiplier tubes are used. By focusing the beam at different tissue depths, three-dimensional images can also be generated. Typical imaging is restricted to depths of a few MFPs owing to diminishing confocal signal with increasing depth, primarily because of scattering.

Whereas 2P/MP microscopy also uses laser-scanning principles, focused femtosecond laser pulses are used for illumination. By concentrating the beam energy in space (focusing) and in time (ultrafast pulses) substantial signal can be generated based on 2P/MP absorption but only within the spatially confined area of the focus point. All fluorescence photons generated therefore come from a highly localized volume. By collecting light generated from scanning a laser beam over an area of interest, one can piece together two- or three-dimensional images as in confocal microscopy. In this case, the photons collected have generally been scattered multiple times because no pinhole is used. In two-photon microscopy, two near-infrared photons (for example, 900 nm) can excite a fluorochrome in the visible spectrum (for example, 450

nm). By collecting all the available light and by using near-infrared excitation light, which is attenuated less than the visible light used for

excitation in confocal microscopy, higher penetration can be achieved in two-photon compared to confocal microscopy[4]. Typical two-photon setups usually achieve worse resolution than that of confocal microscopes because the diffraction-limited focal spots widen as the illumination wavelength increases. When expressed in terms of tissue penetration depth in physical units (millimeters), the depth of two-photon microscopy (which operates in the near-infrared spectral region) is reported as 2–3 times deeper than confocal microscopy (which operates in the visible range). However, this difference is not markedly different when expressed in MFP terms because the MFP is longer for near-infrared than for visible light.

Together, confocal and 2P/MP microscopy have been used extensively for *in vivo* imaging of fluorescent proteins, probes or dyes to investigate structure, function and molecular events as they occur in unperturbed environments[9]. Two-photon imaging currently defines the upper limit of penetration depth in diffraction-limited microscopy, achieving depths of about half a TMFP (**Fig. 2**).

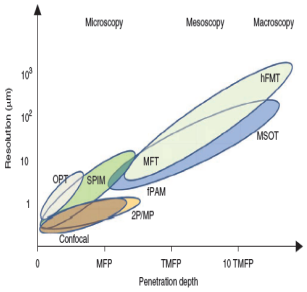

Figure 2 The penetration depth and resolution of modern photonic imaging techniques is depicted. For living tissues, the methods at the left of the graph are primarily limited by light scattering, whereas methods to the right are primarily limited by light attenuation in tissue, a parameter that depends on both absorption and scattering, or by ultrasound attenuation. Although OPT can operate deeper than the MFP range shown, image resolution deteriorates too quickly with increasing MFP to be widely useful. hFMT, hybrid FMT.

Optical projection tomography. Optical visualization is very simple in the absence of light scattering. In transparent media, light propagates through tissue as do X-rays, with the major modifying parameter being absorption of the light. In this case, tomographic approaches similar to those developed for XCT could be used for volumetric optical image reconstruction.

Sharpe *et al.*[10] showed that, instead of accounting for the effects of photon scattering using a physical solution, chemical treatment of the specimen with organic solvents (such as mixture of benzyl alcohol and benzyl benzoate) can be used to optically 'clear' the tissue, that is, to substantially reduce photon scattering and thus produce a transparent specimen10. Imaging is then based on tissue *trans*-illumination over multiple projections, in analogy to XCT measurements, using nonfocused light beams. The images collected serve as raw data in data inversion algorithms similar to those used in XCT, which reconstruct a three-dimensional image of the sampled volume. This method, termed optical projection tomography (OPT), offers an alternative approach to obtaining three-dimensional images of large samples such as small animal embryos and organs. The chemical treatment is toxic, however, and therefore only appropriate for postmortem imaging.

OPT penetration is essentially limited by the penetration ability of the various chemicals into tissue and how effectively they can reduce scattering, not by the physical components of the imaging system. The method can be applied to image fluorescence, using tissues expressing fluorescent proteins or stained with dyes, or to image optical absorption of the tissue, in analogy to tissue attenuation imaging by XCT. In the original work, a simple back-projection algorithm was used for image reconstruction10, but theoretical correction of the actual lines of sight in the optical system was suggested for improving imaging performance[11]. The images generated by OPT accurately capture three-dimensional structures in the tissues studied and have the advantage that they do not alter morphological characteristics as may be the case when physical tissue sectioning is used. The method has been applied to imaging mouse embryos in different development stages, limb development and the morphologies of different organs[12–14].

OPT does not correct for tissue scattering and therefore operates theoretically under the same depth limitations as conventional microscopy, within the 0.1–0.2 MFP range. In uncleared samples, the method is therefore limited by a 10–20-µm penetration limit before photon scattering blurs the resulting images. Therefore, OPT is ideally suited for imaging cleared or otherwise naturally transparent specimens. OPT imaging deeper than 0.2 MFP is possible and has been applied to uncleared samples *in vivo*, for example, in imaging growing mouse limb buds[14], but in this case the corresponding images appear blurred in analogy to microscopy using slices that are thicker than 10–20 µm.

Selective plane illumination microscopy. Also pursuing the goal of easy-to-implement microscopic imaging of large

samples, Huisken *et al.*[15] developed an approach that captures volumetric images of a specimen using illumination that is shaped by a cylindrical lens to form a thin plane of light (light sheet). This light plane is established orthogonal to the detection axis and therefore only partially illuminates the tissue of interest (Fig. 3), in contrast to OPT or conventional microscopy in which the entire specimen is illuminated. Image formation is then based on piecing together raw images, each collected after translating or rotating the sample in relation to the light plane, in a step-wise manner that scans the entire volume of interest. As slice selection is performed optically, a reconstruction method such as the back-projection method in OPT is not necessarily required. This technique, termed selective plane illumination microscopy (SPIM) also has limitations owing to light scattering as do conventional microscopy or OPT, but it is less susceptible to its effects because the volume of interest is only partially illuminated, thereby producing less scattered photons compared to OPT, which illuminates the entire volume of interest in each projection. SPIM has been shown to image with 6-µm resolution up to a depth of about 500 µm (~1–2 MFP) in semitransparent medaka fish, attaining resolution improvements over volumetric tissue illumination[15].

When imaging beyond a few MFP tenths, detected light will scatter as it propagates through tissue and will blur the corresponding images. Scattering also complicates the establishment of a well-defined light-plane for depths beyond a few MFP tenths. To improve imaging performance, illumination from opposite directions into the sample has been used, doubling the light penetration in a small specimen[16]. Image deconvolution was shown to additionally improve SPIM performance and resolution[17]. Similarly to OPT, SPIM has also been combined with methods for tissue clearance[18], achieving optical penetration of up to 2 mm in the brain of mouse embryos and of 400 µm or better in 35-day-old transgenic GFP-expressing mice[19].

SPIM offers a practical and economic implementation for volumetric imaging within a few MFP and can be integrated with a conventional microscope for three-dimensional visualization, although not at diffraction-limited resolution (as in confocal or 2P/MP microscopy) for depths approaching 1 MFP and beyond.

Optoacoustic microscopy. Optoacoustic (also termed photoacoustic) methods are emerging as powerful approaches for imaging optical absorption in tissues. The principle of operation is based on resolving the origin of ultrasound waves, in the 1–100 MHz range, generated in response to short nanosecond-range light pulses propagating through tissue[20,21]. The ultrasound waves are generated by the transient thermoelastic expansion of light-absorbing structures, following transient local temperature rise owing to molecules that absorb energy from the photon pulse. Optoacoustics essentially 'listen' to the absorption of light by tissue components and relate the acoustic signal to a corresponding absorption property[22].

Using optoacoustics, Zhang *et al.*[23] devised an approach termed functional photoacoustic microscopy (fPAM) that operates in the microscopic regime. In fPAM, tissue is illuminated with a short (a few nanoseconds) laser pulse focused with a conical lens to an area in tissue that coincides with the focal point of a wideband ultrasonic detector. The optoacoustic responses generated from tissue are then detected with the acoustic detector. fPAM has been used to image functional and structural contrast in tissues, such as that of blood vessels and blood oxygenation. However, it is possible to use such an approach for molecular imaging of optical reporters such as fluorochromes, chromophoric molecules or nanoparticles by using multispectral principles[24] as described in the "Multispectral optoacoustic tomography" section below.

In fPAM, acoustic rather than optical signals are detected; this is a distinct difference from laser scanning confocal microscopy. The laser focus in fPAM can be intentionally kept wider than the ultrasonic focal point, so that the entire volume of the ultrasonic focal zone is adequately illuminated. In this case, the fPAM resolution does not tightly depend on tissue scattering characteristics because it is not the light focusing ability but the numerical aperture and the frequency response of the ultrasonic detector that determine the resolution of the method within a few MFPs to a few TMFPs. Correspondingly, fPAM achieved ~10-µm resolution at depths <1 TMFP23. However the resolution degraded to 120 µm within 1.2 mm of skin penetration, likely because of increased ultrasonic attenuation[25]. Nevertheless, fPAM can offer substantial flexibility in visualizing optical contrast at greater depths than other optical microscopy methods with ~10–20-µm resolution. Higher lateral resolution is also possible in fPAM, when focusing light tighter than the ultrasonic focal zone dimensions, but in this case the image resolution as a function of penetration depth generally obeys the light scattering limitations. For example, fPAM demonstrated 5-µm lateral resolution within ~1 MFP of mouse ear tissue when using a tightly focused laser beam for illumination[26]. In this implementation, axial resolution was determined by the frequency response of the ultrasound transducer to be 15 µm.

As in confocal or 2P/MP microscopy, fPAM images are generated from raster scans by piecing together information collected from different foci. Reconstruction methods are therefore not required for image formation. However, the detection of ultrasonic waves allows time-

dependent measurements from a depth-resolved line per raster position, in contrast to the single-point detection per raster position in confocal and 2P/MP microscopy. Therefore, in fPAM, three-dimensional images may be generated with two-dimensional scans.

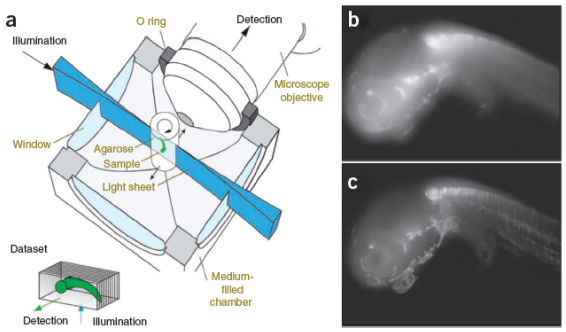

Figure 3 Principle of operation of SPIM. (a) A thin plane of light shaped by a cylindrical lens is used to illuminate the specimen at a plane perpendicular to the optical detection axis. (b,c) Lateral maximum projections in the semitransparent fish medaka using conventional (b) and selective plane illumination (c). A reduction of blurring is evident on the SPIM image compared to the conventional volumetric illumination. The image is adapted from ref. 15; reprinted with permission from the American Association for the Advancement of Science.

Other types of microscopic imaging. There are several microscopic methods in addition to the ones discussed so far, although not all are appropriate for molecular imaging of optical reporters *in vivo*. Optical coherence tomography (OCT)[27,28] illuminates tissue with light of low coherence and detects back-reflected light based on coherence matching between the incident and reflected beams using an interferometric approach. As coherence is essential to the detection process, the method is primarily sensitive to scattering from tissues, as opposed to absorption. In addition, the method cannot be used to resolve fluorescence because fluorescence emission is incoherent in relation to excitation light. Therefore OCT has been primarily considered for anatomical imaging, although methods and nanoparticles that allow molecular sensing in OCT have been reported as well[29–32].

Although the technologies described so far describe the major approaches to reduce the effects of scattering on detected light and thus on the corresponding images, considerable gains in microscopy are also achieved by contrast-enhancement approaches. Fluorescence resonance energy transfer, fluorescence recovery after photobleaching, fluorescence loss in photobleaching, fluorescence lifetime microscopy, higher-order optical harmonic generation and coherent anti-Stokes Raman scattering are all approaches based on mechanisms that, though they do not change the resolution or penetration depth of microscopy, allow different structural, functional, biochemical or molecular parameters to be detected[33–48]. This is achieved by capturing contrast associated with different biochemical parameters of the molecules involved in image generation. These methods expand the application of microscopy to diverse biological fields, spanning the visualization of cellular and subcellular structures, the diffusion and binding characteristics of molecules, protein-protein interactions and several other, otherwise invisible, cellular events. Several of these methods can be implemented using a conventional or laser-scanning microscope and can drastically improve its visualization capacity.

Macroscopy: the power of hybrid imaging

Macroscopy, defined here as imaging beyond the 10 TMFP range (in tissue, this typically translates to >1 cm), is associated with visualization of human tissues or entire animals. Optical macroscopy has been two decades in development toward quantitative *in vivo* imaging[49,50] but has only recently reached a performance maturity allowing for accurate and high-resolution imaging of tissue biomarkers. This has occurred via the development of imaging methods that accurately account for the diffusive nature of photons beyond the 10 TMFP range and because of the availability of improved optical reporters[6,33,51–53]. Macroscopic optical imaging was initially performed with stand-alone systems[22]. Recently, the development of optoacoustic imaging or systems that combine an optical system with MRI or XCT have led to hybrid implementations that substantially improve the imaging performance and that potentially have many more applications compared to the original optical implementations.

Whereas photon scattering in tissue imposes the dominating limitation for microscopy and also reduces the resolution for macroscopy, penetration depth limits for macroscopy are defined by light attenuation in tissue, which depends both on tissue scattering and on tissue absorption. This leads to loss of sufficient signal at 3–6 cm depth in muscle or brain or at 10–12 cm depth in less absorbing organs such as the human breast and presents an upper limit of penetration depth for photonic imaging applications[54]. Macroscopic applications can be considered for small animal imaging (mouse and rat), imaging of certain organs such as the breast in larger animals and humans or in endoscopic and intraoperative applications.

Hybrid fluorescence molecular tomography.
Fluorescence molecular tomography (FMT) is a diffuse optical tomography technique developed to three-dimensionally and quantitatively image the biodistribution of fluorescence in small animals and tissues through several TMFPs55. The method uses optical illumination of a tissue of interest over multiple angles (projections) and collects photons that have propagated through tissue, over different spectral bands, typically fluorescence (emission) photons and excitation photons. The mathematical processing of the raw data yields three-dimensional quantitative images of the distribution of fluorescent reporters in tissue[56].

The major differences between FMT and tomographic techniques in microscopy, such as OPT, are that in FMT (i) point light sources are used to illuminate the tissue surface, as this can improve the resolution achieved in diffusive media[50] and (ii) image reconstruction is based on different theoretical models and assumptions of photon propagation than the ones used in OPT. Despite the use of elaborate inversion methods and point sources, scattering leads to challenging (ill-posed) image reconstruction problems and effectively limits the resolution (1 mm to 1 cm) and the quantification accuracy achieved.

To improve on the performance of macroscopic optical tomography methods such as FMT, the implementation of systems that combine the optical method with high-resolution anatomical methods has been suggested since the mid-1990s[57–59]. The resulting hybrid system[60–62] can use data from the high-resolution modality to improve the optical reconstruction algorithm, yielding more accurate images than the ones produced by stand-alone approaches. Hybrid FMT imaging can be implemented by imaging the sample placed within a common hybrid system[60,61,63,64], potentially allowing simultaneous imaging or by using rigid translation systems (for example, a common animal holder) that allow consecutive imaging in different systems under identical sample placement conditions and using postprocessing to align the datasets from the two modalities65. The information from anatomical images, referred to as 'image priors', can be used in two ways: (i) to improve the accuracy of the photon propagation (forward) model and (ii) to restrict the inversion procedure to meaningful solutions, that is, to reduce the uncertainty of the inverse problem. It is, however, important that the 'image prior' information is used in such a way that it does not bias the solution[65–67].

The use of prior information from XCT in the inverse FMT problem has been shown61,65 (Fig. 4a–g). A 24-month-old *APP23* (B6,D2-Tg(Thy1APP)23/1Npa) transgenic mouse, which developed amyloid-beta plaques similar to the ones seen in human Alzheimer's disease, was imaged using XCT and FMT. The mouse was injected with a fluorescent oxazine dye for *in vivo* staining of the plaques[68]. The reconstruction without the use of X-ray priors was compared to that with priors (Fig. 4d,e), demonstrating the imaging improvement achieved. *Ex vivo* widefield epi-illumination fluorescence imaging (Fig. 4f), performed immediately after *in vivo* imaging, showed good congruence between the *in vivo* findings and the fluorescence bio-distribution confirmed *ex vivo*. Figure 4h–k illustrates results from the use of priors in clinical breast imaging of hemoglobin content, using hybrid MRI and optical tomography[61]. Although the images in this case do not resolve fluorescence, the example showcases the clinical propagation of the use of priors in optical tomography problems.

Hybrid systems may impose imaging compromises, for example, when the optical system is mounted in small bores, typical of MRI systems, which may require fiber coupling or low-performance magnetic resonance–compatible cameras to be used, allowing a limited number of sources and detectors[60]. Technological advances may improve data collection in the future. However, in other implementations, such as in XCT, a fully capable optical imaging system can be engineered onto the rotating gantry using direct coupling of high-performance charge-coupled device (CCD) cameras[64].

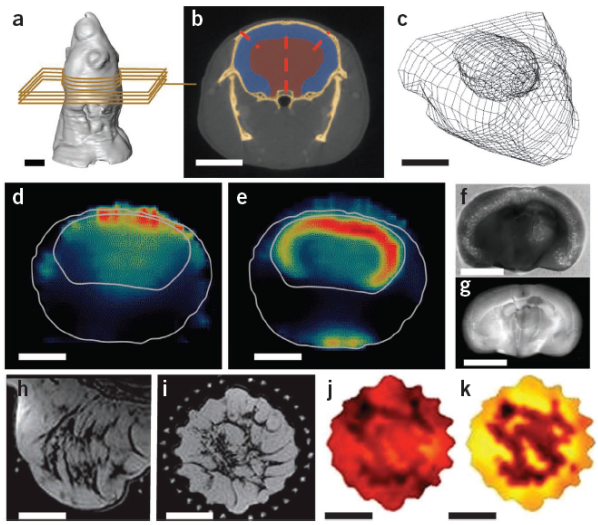

Figure 4 Hybrid optical tomography using priors. (a–c) Surface rendering of XCT volumetric data from an *APP23* transgenic mouse (a) that are segmented (b) and used to build a three-dimensional mesh geometry representative of external and internal interfaces (c). (d,e) FMT without the use of priors (d), and hybrid FMT with priors (e), demonstrating imaging improvement. (f) Epifluorescence image obtained *ex vivo* of a brain slice approximately the same as the slice imaged in d and e. (g) *Ex vivo* reflection image of the same brain slice. Data are modified from ref. 65; reprinted with permission from Elsevier. Scale bars, 4 mm (a–g). (h–k)

Optical images generated with priors from the breast of a healthy individual, imaged by axial (h) and coronal (i) T1-weighted MRI, which was used as an image prior to build accurate reconstructions, yielding images of hemoglobin concentration (j) and oxygen saturation (k) in the breast. Scale bar, 4 cm (h–k). Data are modified from ref. 61; copyright (2006), National Academy of Sciences, U.S.A.

Multispectral optoacoustic tomography. Macroscopic detection of optical reporters has also been shown to be possible using multispectral optoacoustic tomography (MSOT) (Fig. 5a,b). In contrast to fPAM, the macroscopic implementation of optoacoustic imaging commonly uses expanded light beams that illuminate large tissue areas (Fig. 5a). The method uses photon pulses to establish transient fields of diffusive photons inside the tissue, which, upon absorption, give rise to acoustic waves that can be detected with an array of ultrasonic detectors placed around the sample (Fig. 5b). Tomographic reconstruction in this case is based on mathematical inversion methods, using a model of acoustic and possibly of photon propagation in tissue[21,69,70]. Macroscopic optoacoustic sensing and imaging of intrinsic tissue chromophores has been described since the 1980s[71] and has more recently been shown to be capable of imaging blood vessels and oxy- and deoxy-hemoglobin[21,72–75]. Measurements at multiple wavelengths enable molecular imaging applications as well, by identifying the spectral signatures of optical reporters such as chromophores, fluorochromes or nanoparticles, over the background tissue absorption[24].

The resolution in macroscopic optoacoustic tomography is not limited by tissue scattering but by the attenuation of acoustic frequencies by tissue (it is stronger for higher frequencies, which contribute to high spatial resolution). The resolution therefore also drops with depth, but at a slower rate compared to purely optical imaging methods, yielding resolutions of the order of ~50–200 µm for imaging at depths of 10 TMFPs or more. Light scattering, together with optical absorption, contributes to the overall light attenuation, which dictates the penetration depth of optoacoustics.

A major challenge of MSOT is achieving accurate quantification, as light distribution through several TMFPs in tissue is not homogeneous. Light intensity depends nonlinearly on depth and on spatial variations in tissue absorption and scattering. As a result, considerable photon field intensity variations may be present, resulting in intensity variations in the corresponding optoacoustic image and limiting quantification and accurate image formation. Similarly, acoustic attenuation may also lead to quantification and image-fidelity limitations.

A particular advantage of MSOT over single-wavelength optoacoustic measurements is that the information contained at multiple wavelengths can be used to improve the accuracy of the reconstructed images as a function of depth. A subset of the spectral measurements can estimate or correct the photon attenuation in tissue for measurements at adjacent wavelengths[56]. Spectral approaches that account for optoacoustic intensity variations owing to inhomogenous light distribution are now emerging[76,77] and can be important in yielding accurate MSOT performance. Another distinct feature of MSOT over conventional optoacoustic imaging is that, owing to the spectral separation of the optical reporter of interest from background absorption, there is no need to obtain baseline measurements, that is, images obtained before the administration or expression of a chromophoric molecular probe[24]. This is particularly important in applications in which such baseline measurements may not be possible because of long circulation or clearance times of administered probes or unknown expression patterns of reporter genes.

Optoacoustic imaging offers a versatile platform for various molecular imaging applications. MSOT imaging of fluorochromes has been demonstrated in animal tissues[24,78,79] (Fig. 5c–j) and in nonabsorbing phantoms using a dual-wavelength approach[80]. The methods typically use tunable nanosecond lasers such as pumped pulsed optical parametric oscillators. MSOT can achieve fast, video-rate imaging for a given wavelength, in analogy to ultrasound. With progress in wavelength switching technology, 2–4-wavelength scans could also be implemented to achieve multiwavelength video-rate scans. The images shown in Figure 5g–j were obtained with a method termed spectral photoacoustic tomography (SPAT), an alternative term to MSOT, although in this implementation tissue was illuminated from a single angle, which is appropriate only for imaging superficial events. In this case a homogenous photon intensity distribution into the sample was assumed, a practical approximation close to the tissue surface. Gold nanoshells, nanoparticles and nanorods, some conjugated to monoclonal antibodies[33,75,81], targeted single-walled carbon nanotubes[53], β-galactosidase expression[82], quantum dots[52] or dual approaches using magnetic and carbon nanotubes have also been considered for molecular optoacoustic imaging *in vivo*[83].

The emerging mesoscopic regime

Mesoscopic imaging of cellular and subcellular optical reporters remains in its infancy. Most researchers performing *in vivo* imaging in the mesoscopic (1–10 TMFP) regime are limited to studying naturally transparent biological organisms or to postmortem studies using histology. The core technologies involved in optical

mesocopy are not fundamentally different from those used in macroscopy, but certain adaptations are required for optimal operation on the smaller scales involved. First, mathematical solutions used for modeling wave propagation in tissues at macroscopic scale may not be appropriate for imaging in the sub–10 TMFP range. Second, because mesoscopy requires higher resolution and smaller field of view, it generally needs different hardware and operational characteristics, for example, more precise geometrical implementations, or higher frequencies in terms of spatial sampling or frequency detection bandwidth compared to macroscopy.

Mesoscopic molecular imaging enables longitudinal *in vivo* observations of small nontransparent animals with applications in developmental and mutagenesis studies. *In vivo* visualization of fluorescence proteins can reduce the need for laborious histological analyses of multiple organisms at different time points. Instead, *in vivo* mesoscopic imaging can be used to guide histological intervention when important conformational or functional changes are observed *in vivo*. Through nondestructive longitudinal studies, mesoscopy may enable observation of fast, transient events that are difficult to capture by histological sampling and eliminate artifacts that could be due to the histological treatment itself.

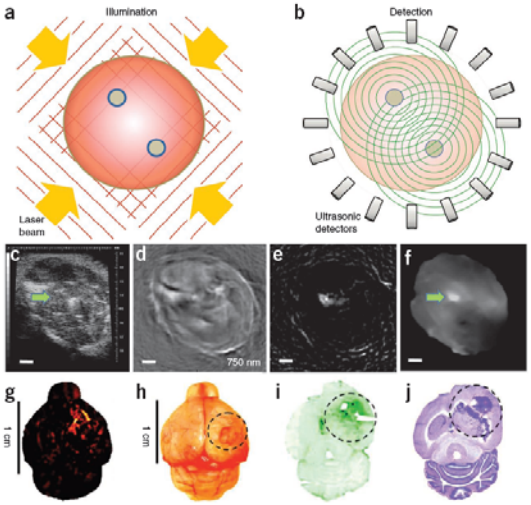

Figure 5 Principle of operation of volumetric optoacoustic tomography. (**a**) An ideal tissue (large circle) with two circular absorbing structures is illuminated by expanded laser beams operating as pulses in the nanosecond range. (**b**) In response to the pulsed tissue illumination, an optoacoustic signal is generated by the absorbers, which is then peripherally detected by ultrasonic detectors. Mathematical inversion methods are then used for image reconstruction. (**c**) Ultrasound image of a mouse leg injected with Alexa Fluor 750 dye approximately at the area shown by the arrow. (**d**) Optoacoustic absorption image obtained at a single wavelength (750 nm); images in **c** and **d** were obtained from the same leg under similar but not identical placement positions. (**e**) MSOT image of the AF 750 dye, obtained using three wavelengths (750, 770 and 790 nm) with a 3.7-MHz transducer, achieving 150-µm resolution, under identical placement as in **d**, resolving the fluorochrome with high specificity. (**f**) Epi-illumination fluorescence image from a slice taken after dissecting the mouse leg imaged noninvasively in **c**–**e**. Scale bars, 1 mm. Modified from ref. 24; reprinted with permission from the Optical Society of America. (**g**–**j**) Optoacoustic imaging of a U87 glioblastoma in mouse brain *in vivo* 20 h after intravenous injection of a fluorescent probe targeting avb3-integrin. Shown are an optoacoustic *in vivo* image of probe biodistribution (**g**), a photograph of the excised brain, and (**h**) fluorescence image (**i**) and thionine-stained (**j**) brain sections imaged 1 mm below the brain cortex (dotted circles indicate the approximate position of the glioblastoma). Scale bars, 1 cm (**g**,**h**) and (**i**,**j**). Images were modified from ref. 78; reprinted with permission.

Mesoscopic fluorescence tomography. For imaging around and beyond 1 TMFP, mesoscopic fluorescence tomography (MFT)84 was recently shown. MFT is similar to OPT in that volumetric tissue illumination is accomplished with an incident light field at multiple projections and a CCD camera with a lens collects the transmitted fluorescence signals from the tissue. In contrast to OPT, however, MFT uses mathematical models of photon propagation in tissue to model the forward scattering that occurs around 1 TMFP. By then using appropriate inversion theory and by modeling refraction effects at the air-tissue interface, images of the internal structures of nontransparent organisms can be produced. Application to studies of *Drosophila melanogaster* morphogenesis demonstrated that dynamic three-dimensional visualization of internal structures is possible with MFT, confirmed by histology at select time points (Fig. 6). In contrast, when using algorithms used in OPT (assumption of no scattering) or in FMT (assumption of fully diffusive photons), it was not possible to reconstruct meaningful images[84].

Mesoscopic optoacoustic imaging. In optoacoustics, the transition between macroscopy, mesoscopy and even microscopy is rather continuous (Fig. 2). From a technology standpoint, optoacoustic macroscopy methods such as MSOT can be adapted for mesoscopic imaging by using detectors of higher central frequency and wider bandwidth (10–80 MHz) and by using different photon propagation assumptions. Likewise, microscopy methods such as fPAM can be extended into the mesoscopic regime at the expense of the resolution achieved. Therefore, optoacoustics are ideally suited for the mesoscopic regime. Mesoscopic MSOT was recently accomplished in adult zebrafish using multiprojection volumetric illumination (in analogy to OPT or MFT) and multiprojection acoustic detection[85] (Fig. 6b–e). The method also incorporated light-sheet illumination, using a cylindrical lens to concentrate the excitation energy into the slice of interest, which improved scanning times and overall image quality over unfocused methods. The authors visualized structures expressing fluorescent proteins in the adult zebrafish and

developing *Drosophila in vivo*. As in macroscopic MSOT, the resolution in this case was not limited by photon scattering in tissues but by the acoustic detector characteristics. In this study the imaging system used a detector with a central acoustic frequency and bandwidth of 15 MHz and 3.5 MHz, respectively, achieving 38-µm resolution through at least 6 mm of adult, nontransparent zebrafish. As noted, however, it is possible to exchange penetration depth for resolution and vice versa. They also found that although mesoscopic fluorescence tomography performs with higher resolution at around 1 TMFP, mesoscopic MSOT was the method of choice for 2 TMFP and beyond[85].

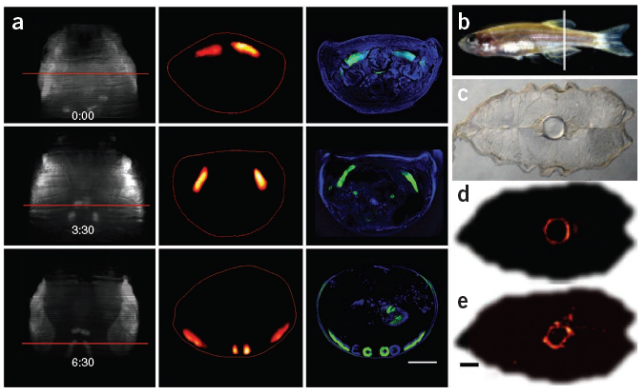

Figure 6 Examples of mesoscopic imaging. (a) Time-lapse imaging (hours:minutes) of the *Drosophila* pupa wing imaginal disc. Shown are *trans*-illumination fluorescence images of GFP expressed in the wing discs of a single live pupa (left), MFT of slices reconstructed from the planes indicated by red lines on the left, after inversion of measurements obtained over 360° projections (middle), and corresponding histological slices stained with DAPI from different pupae, taken from approximately the same time points as the *in vivo* images (right). Scale bar, 300 µm. Images were modified from those in ref. 84; reprinted with permission from Nature. (b–e) Mesoscopic MSOT imaging of the fluorescent protein mCherry expression in the notochord of a transgenic adult zebrafish (b); the location of the imaging plane is indicated by the white line. (c,d) Histological section (c) and epi-fluorescence image (d) of dissected tissue from the imaging plane (red corresponds to mCherry-expressing notochord). (e) MSOT image obtained *in vivo* from the imaging plane. Scale bar, 400 µm. Images were modified from those in ref. 85; reprinted with permission from Nature.

Comparative performance

Operational characteristics. Two important imaging parameters are resolution and penetration depth, and these essentially direct the applications for each imaging method. A third important parameter is detection sensitivity, which depends on the imaging depth, the time allowed for image acquisition and on the particular technology used. Acquisition speed can usually be exchanged for sensitivity, by increasing the time over which the data are captured to increase the intensity of the signal, but this comes with a loss of temporal resolution, which is important for imaging dynamic events. Generally, purely optical methods appear to be of higher sensitivity than optoacoustic methods, at least in macroscopy studies, although there have been so far no conclusive comparative studies of these methods. Optical methods typically report nanomolar sensitivity[22] (~100–500 femtomoles) for organic dyes in mice whereas optoacoustic methods report micromolar sensitivity, although this performance can be improved via the use of agents with high absorption cross-section[53], most notably gold and carbon nanoparticles. Microscopy methods can also make use of a wider spectrum of contrast enhancement techniques as described. Conversely, photobleaching and possibly tissue photodestruction become concerns in microscopy because light beams are focused in diffraction-limited volumes unlike in methods used for imaging deeper in tissue. Finally, different methods differ from one another in terms of implementation complexity and cost. Performance characteristics are summarized in Table 2.

Another important classification of *in vivo* imaging methods, independent of the dimensions at which they operate, separates them into scanning techniques, with which the raw data are used directly to generate images, and reconstruction methods, with which the raw data are fed into inversion algorithms for image formation, even if scanning is done to generate the data. Typically, the microscopic methods described here are scanning techniques, with the exception of OPT, which uses image-reconstruction principles.

Scanning refers to the process of sequentially collecting raw data during translation or rotation of the illumination and detection paths in relation to the specimen, as in confocal and two-photon microscopy or SPIM. For SPIM, in contrast to laser scanning microscopy in which one point at a time is collected, two-dimensional arrays of virtual slices through tissue are collected. Each of the raw data images thus represents one plane in space. The image formation algorithm in this case creates a three-dimensional matrix, representative of the corresponding volume imaged and populates it using the raw data measurements. A form of interpolation or linear transformation may then be required—for example, to convert from a system of polar coordinates to Cartesian coordinates. Finally, image-processing tools may be applied to reduce noise and for visualization and rendering purposes.

Image reconstruction methods operate on markedly different principles. Typically, the collected data represent responses not from single points or planes in space but rather from entire volumes in the tissue of interest. Reconstruction-based methods require projections, that is,

object illumination or data collection from different view angles. To produce an image, one needs to use a mathematical model of energy propagation in tissue. This mathematical model, termed the 'forward model', can be used to calculate the expected raw data, given that the experimental parameters and the geometrical and optical and/or acoustic properties of the object of interest are known. Then, for retrieving an image of an unknown object in the presence of measured data an 'inverse model' is used, by which an image of the unknown object is calculated so that it matches the experimental measurements. The final image can also be filtered and processed for rendering purposes. FMT presents the most challenging inverse problem, because of the uncertainty in the data on account of photon diffusion; this can, however, be improved by using priors. Data from other tomographic methods can be inverted with better certainty, although each method presents unique problems as discussed in the corresponding sections.

Table 2 Summary of performance characteristics

	Resolu-tion (μm)	Pene-tration depth	Sensi-tivity	Photo-toxicity	Cost /comple xity	Inver-sion (versus scan)
Confocal	<1	2–3 MFP	<nM	+++	++	No
2P/MP	<1	3–4 MFP	<nM	+++	+++	No
OPT	~1–10	~0.2 MFPb	<nM	++	+	Yes
SPIM	0.5–10	<1 MFP	<nM	++	+	No
fPAM	5–20	~1 MFP to few TMFP	nM	++	+++	No
MFT	>20	~1 TMFP	nM	++	+	Yes
MSOTc	>20	>1 TMFP	nM–μM	++	+++	Yes
hFMT	>500	>1 TMFP	nM	+	++	Yes

aMore plus signs indicate greater cost and/or greater complexity. bOPT can generate images at greater depths than 0.2 MFP but at strongly deteriorating image resolution and fidelity. cMetrics listed for mesoscopic and macroscopic MSOT.

Applications. Photonic imaging methods have diverse performance and operational characteristics and are therefore typically applied for diverse purposes in biological *in vivo* imaging.

Confocal or 2P/MP microscopy permits diffraction-limited longitudinal imaging of tissues *in vivo* (intravital imaging) using invasive procedures such as implantable windows or fiber based catheters and objectives placed on the surface of interest and imaged in epi-illumination mode[86,87]. These methods are preferred for basic biology studies in which cellular and intracellular visualization is required, for instance, to visualize cellular content, cell-cell interactions and angiogenesis in cancer research and to evaluate drug effects[9,88], in neuronal imaging[89,90] or in immunology and physiology studies[91,92]. However, as intravital microscopy operates with small fields of view (~1 mm^2) and superficial depth, it does not yield a complete picture of the underlying activity. For this purpose, mesoscopic and macroscopic imaging may become highly complementary. In addition, OPT and SPIM enable volumetric imaging in a subset of samples, typically small organisms and excised organs, in developmental biology and functional genetics[12,13]. fPAM has been shown so far to be appropriate for blood vessel imaging but could in the future play a major role in the imaging of optical reporters. Mesoscopic imaging, although not yet widely disseminated, may find applications in developmental biology and experimental genetics by allowing the fast and accurate visualization of intact developing organisms. Methods developed for mesoscopy generally enable visualization of larger specimens compared to OPT and SPIM. Mesoscopy could also prove useful in application to arthritis research or in studies of metastasis and lymphatic systems in small animal extremities.

Finally, macroscopy is most apt for noninvasive imaging of entire organs and animals *in vivo*. Its applications include volumetric quantitative imaging, imaging of large fields of view and imaging at sites that are not easily accessed by intravital microscopy, such as the heart and other internal organs. Macroscopy approaches are therefore well suited for visualizing entire tumors, for molecular imaging of cardiovascular disease, for brain imaging applications and for the study of the movement of stem cells or immune cells at deep locations. Owing to sensitivity and resolution restrictions compared to microscopy, however, these approaches are more typically part of drug testing and mouse-to-man clinical translation imaging applications. Another application could be in identifying critical time points during a study and guiding other laboratory analyses, such as conventional invasive histology and immunohistochemistry or *in vivo* microscopy.

Toward a new biological imaging culture

Although microscopy has been a fundamental tool in biological discovery for centuries, the ability to image deeper than a few hundred micrometers is now emerging. This development has followed the relatively recent realization that photons can be used for macroscopic biological observation[93] as well as seminal work offering theoretical models that describe photon propagation in tissues[49]. As discussed here, molecular imaging methods now permit *in vivo* observations in the microscopic, mesoscopic and macroscopic regimes, at depths of a few micrometers to several centimeters, offering a diverse arsenal of tools for biological interrogation.

This ability to accurately visualize beyond the microscopic scale opens up exciting possibilities for a shift in biological observation. The limited penetration depth of optical microscopy has, in part, shaped the use of isolated cells or of naturally transparent biological organisms, such as fish and worms, to draw conclusions about human development, function and disease. Alternatively, histology on excised tissues at isolated time points is often used to study dynamic processes. *In vivo* imaging methods can improve on these established approaches by allowing noninvasive longitudinal observation of dynamic phenomena in their unperturbed environments or the study of species other than naturally transparent organisms. The mesoscopic and macroscopic photonic methods reviewed here now show performances that have evolved considerably over the past decade and may offer an alternative to other established biological imaging methods such as small-animal XCT, MRI, positron emission tomography or single-photon emission tomography. *In vivo* photonic methods intrinsically can be used to image multiple targets simultaneously through spectral differentiation, use nonionizing radiation and have the potential for high dissemination in biological laboratories in the form of mesosopic and macroscopic extensions of the microscopy facility. A major limitation of photonic methods, however, remains their lesser penetration depth compared to MRI or higher-energy photon imaging modalities, making them particularly appropriate for biological interrogations of small animals or select organs in larger animals.

Changing a paradigm shaped by three centuries of microscopic observation will not happen overnight. New *in vivo* approaches must be evaluated against established methods, and the signals produced should be reduced to useful metrics in biological research. In addition, despite the current availability of molecular probes, the development of new *in vivo* staining moieties and strategies will be needed to enhance the application potential of these new methods. Potential clinical applications of these methods can be also foreseen. Surgical, endoscopic and intravascular procedures are all currently based on human vision or simplistic photographic and video-color imaging and could be enhanced by the adaptation of more accurate and deeper penetrating optical molecular imaging methods. Similarly, the availability of high-performance photonic macroscopy with the capacity to operate through centimeters (tens of TMFPs) could impact clinical imaging beyond superficial endoscopic approaches, for example, using dedicated breast cancer or human cortex imaging scanners.

ACKNOWLEDGMENT

I acknowledge investigators and students for their multiple contributions in understanding optical and optoacoustic performance; J. Ripoll for the contribution of Figure 1b; and support from a European Research Council Senior Investigator Award, the German Federal Ministry of Education and Research and the Institute for Biological and Medical Imaging

COMPETING FINANCIAL INTERESTS

The author declares no competing financial interests.

REFERENCES

1. Beauvoit, B., Evans, S.M., Jenkins, T.W., Miller, E.E. & Chance, B. Correlation between the light-scattering and the mitochondrial content of normal-tissues and transplantable rodent tumors. *Anal. Biochem.* 226, 167–174 (1995).
2. Webb, R.H. Theoretical basis of confocal microscopy. *Methods Enzymol.* 307, 3–20 (1999).Aconcise description of confocal microscopy technology and performance metrics.
3. Denk, W., Strickler, J.H. & Webb, W.W. Two-photon laser scanning fluorescence microscopy. *Science* 248, 73–76 (1990).An introduction of two-photon laser scanning fluorescence microscopy.
4. Helmchen, F. & Denk, W. Deep-tissue two-photon microscopy. *Nat. Methods* 2, 932–940 (2005).
5. Tsien, R.Y. Building and breeding molecules to spy on cells and tumors. *FEBS Lett.* 579, 927–932 (2005).Aconcise review of fluorescence reporters and probes for *in vivo* imaging.
6. Weissleder, R. & Pittet, M. Imaging in the era of molecular oncology. *Nature* 452, 580–589 (2008).
7. Stephens, D.J. & Allan, V.J. Light microscopy techniques for live cell imaging. *Science* 300, 82–86 (2003).
8. Zipfel, W.R., Williams, R.M. & Webb, W.W. Nonlinear magic: multiphoton microscopy in the biosciences. *Nat. Biotechnol.* 21, 1368–1376 (2003).
9. Jain, R.K. Normalization of tumor vasculature: An emerging concept in antiangiogenic therapy. *Science* 307, 58–62 (2005).
10. Sharpe, J. *et al.* Optical projection tomography as a tool for 3D microscopy and gene expression studies. *Science* 296, 541–545 (2002).An introduction of optical projection tomography.
11. Walls, J.R., Sled, J.G., Sharpe, J. & Henkelman, R.M. Resolution improvement in emission optical projection tomography. *Phys. Med. Biol.* 52, 2775–2790 (2007).
12. Alanentalo, T. *et al.* High-resolution three-dimensional imaging of islet-infiltrate interactions based on optical projection tomography assessments of the intact adult mouse pancreas. *J. Biomed. Opt.* 13, 054070 (2008).
13. Kerwin, J. *et al.* 3 dimensional modelling of early human brain development using optical projection tomography. *BMC Neurosci.* 5, 27 (2004).
14. Boot, M.J. *et al. In vitro* whole-organ imaging: 4D quantification of growing mouse limb buds. *Nat. Methods* 5, 609–612 (2008).
15. Huisken, J., Swoger, J., Del Bene, F., Wittbrodt, J. & Stelzer, E.H.K. Optical sectioning deep inside live embryos by selective plane illumination microscopy. *Science* 305, 1007–1009 (2004).An introduction of selective plane illumination microscopy.
16. Huisken, J. & Stainier, D.Y. Even fluorescence excitation by multidirectional selective plane illumination microscopy (mSPIM). *Opt. Lett.* 32, 2608–2610 (2007).

17. Verveer, P.J. *et al.* High-resolution three-dimensional imaging of large specimens with light sheet-based microscopy. *Nat. Methods* 4, 311–313 (2007).
18. Dodt, H.U. *et al.* Ultramicroscopy: three-dimensional visualization of neuronal networks in the whole mouse brain. *Nat. Methods* 4, 331–336 (2007).
19. Ermolayev, V. *et al.* Ultramicroscopy reveals axonal transport impairments in cortical motor neurons at prion disease. *Biophys. J.* 96, 3390–3398 (2009).
20. Andreev, V.G., Karabutov, A.A. & Oraevsky, A.A. Detection of ultrawide-band ultrasound pulses in optoacoustic tomography. *IEEE Trans. Ultrason. Ferroelectr. Freq. Control* 50, 1383–1390 (2003).
21. Wang, X. *et al.* Noninvasive laser-induced photoacoustic tomography for structural and functional in vivo imaging of the brain. *Nat. Biotechnol.* 21, 803–806 (2003).Ademonstration of blood-vessel imaging using optoacoustic (photoacoustic) tomography.
22. Ntziachristos, V., Ripoll, J., Wang, L.H.V. & Weissleder, R. Looking and listening to light: the evolution of whole-body photonic imaging. *Nat. Biotechnol.* 23, 313–320 (2005).
23. Zhang, H., Maslov, K., Stoica, G. & Wang, L.V. Functional photoacoustic microscopy for high-resolution and noninvasive *in vivo* imaging. *Nat. Biotechnol.* 24, 848–851 (2006).An introduction of functional photoacoustic microscopy.
24. Razansky, D., Vinegoni, C. & Ntziachristos, V. Multispectral photoacoustic imaging of fluorochromes in small animals. *Opt. Lett.* 32, 2891–2893 (2007).
25. Maslov, K., Stoica, G. & Wang, L. In vivo dark field reflection-mode photoacoustic microscopy. *Opt. Lett.* 30, 625–627 (2005).
26. Maslov, K., Zhang, H., Hu, S. & Wang, L. Optical-resolution photoacoustic microscopy for in vivo imaging of single capillaries. *Opt. Lett.* 33, 929–931 (2008).
27. Huang, D. *et al.* Optical coherence tomography. *Science* 254, 1178–1181 (1991).
28. Tearney, G.J. *et al.* In vivo endoscopic optical biopsy with optical coherence tomography. *Science* 276, 2037–2039 (1997).
29. Bredfeldt, J.S., Vinegoni, C., Marks, D.L. & Boppart, S.A. Molecularly sensitive optical coherence tomography. *Opt. Lett.* 30, 495–497 (2005).
30. Skala, M.C., Crow, M.J., Wax, A. & Izatt, J.A. Photothermal optical coherence tomography of epidermal growth factor receptor in live cells using immunotargeted gold nanospheres. *Nano Lett.* 8, 3461–3467 (2008).
31. Sarunic, M.V., Applegate, B.E. & Izatt, J.A. Spectral domain second-harmonic optical coherence tomography. *Opt. Lett.* 30, 2391–2393 (2005).
32. Drexler, W. & Fujimoto, J.G. State-of-the-art retinal optical coherence tomography. *Prog. Retin. Eye Res.* 27, 45–88 (2008).
33. Chamberland, D. *et al.* Photoacoustic tomography of joints aided by an Etanercept-conjugated gold nanoparticle contrast agent—an ex vivo preliminary rat study. *Nanotechnology* 19, 095101 (2008).
34. Tolentino, T.P. *et al.* Measuring diffusion and binding kinetics by contact area FRAP. *Biophys. J.* 95, 920–930 (2008).
35. McNally, J.G. Quantitative FRAP in analysis of molecular binding dynamics in vivo. *Methods Cell Biol.* 85, 329–351 (2008).
36. Mavrakis, M., Rikhy, R., Lilly, M. & Lippincott-Schwartz, J. Fluorescence imaging techniques for studying *Drosophila* embryo development. *Curr. Protoc. Cell Biol.* 4, 18 (2008).
37. Sprague, B.L., Pego, R.L., Stavreva, D.A. & McNally, J.G. Analysis of binding reactions by fluorescence recovery after photobleaching. *Biophys. J.* 86, 3473–3495 (2004).
38. Provenzano, P.P., Eliceiri, K.W. & Keely, P.J. Multiphoton microscopy and fluorescence lifetime imaging microscopy (FLIM) to monitor metastasis and the tumor microenvironment. *Clin. Exp. Metastasis* 26, 357–370 (2008).
39. Hallworth, R., Currall, B., Nichols, M.G., Wu, X. & Zuo, J. Studying inner ear protein-protein interactions using FRET and FLIM. *Brain Res.* 1091, 122–131 (2006).
40. Chen, Y., Mills, J.D. & Periasamy, A. Protein localization in living cells and tissues using FRET and FLIM. *Differentiation* 71, 528–541 (2003).
41. Tadrous, P.J. Methods for imaging the structure and function of living tissues and cells: 2. fluorescence lifetime imaging. *J. Pathol.* 191, 229–234 (2000).
42. Bastiaens, P.I. & Squire, A. Fluorescence lifetime imaging microscopy: spatial resolution of biochemical processes in the cell. *Trends Cell Biol.* 9, 48–52 (1999).
43. Rodriguez, L.G., Lockett, S.J. & Holtom, G.R. Coherent anti-stokes Raman scattering microscopy: a biological review. *Cytometry A* 69, 779–791 (2006).
44. Rinia, H.A., Wurpel, G.W. & Muller, M. Measuring molecular order and orientation using coherent anti-stokes Raman scattering microscopy. *Methods Mol. Biol.* 400, 45–61 (2007).
45. Cheng, J.X. Coherent anti-Stokes Raman scattering microscopy. *Appl. Spectrosc.* 61, 197–208 (2007).
46. Imanishi, Y., Lodowski, K.H. & Koutalos, Y. Two-photon microscopy: shedding light on the chemistry of vision. *Biochemistry* 46, 9674–9684 (2007).
47. Botvinick, E.L. & Shah, J.V. Laser-based measurements in cell biology. *Methods Cell Biol.* 82, 81–109 (2007).
48. Campagnola, P.J. & Loew, L.M. Second-harmonic imaging microscopy for visualizing biomolecular arrays in cells, tissues and organisms. *Nat. Biotechnol.* 21, 1356–1360 (2003).
49. Patterson, M.S., Chance, B. & Wilson, B.C. Time resolved reflectance and transmittance for the noninvasive measurement of tissue optical-properties. *Appl. Opt.* 28, 2331–2336 (1989).
50. Arridge, S.R. Optical tomography in medical imaging. *Inverse Probl.* 15, R41–R93 (1999).
51. Shu, X. *et al.* Mammalian expression of infrared fluorescent proteins engineered from a bacterial phytochrome. *Science* 324, 804–807 (2009).
52. Shashkov, E., Everts, M., Galanzha, E. & Zharov, V. Quantum dots as multimodal photoacoustic and photothermal contrast agents. *Nano Lett.* 8, 3953–3958 (2008).
53. De La Zerda *et al.* Carbon nano-tubes as photoacoustic molecular imaging agents in living mice. *Nat. Nanotechnol.* 3, 557–562 (2008).
54. Weissleder, R. & Ntziachristos, V. Shedding light onto live molecular targets. *Nat. Med.* 9, 123–128 (2003).
55. Ntziachristos, V., Tung, C.H., Bremer, C. & Weissleder, R. Fluorescence molecular tomography resolves protease activity *in vivo*. *Nat. Med.* 8, 757–760 (2002).An introduction of fluorescence molecular tomography.
56. Ntziachristos, V. & Weissleder, R. Experimental three-dimensional fluorescence reconstruction of diffuse media using a normalized Born approximation. *Opt. Lett.* 26, 893–895 (2001).
57. Schwaiger, M., Ziegler, S. & Nekolla, S. PET/CT: challenge for nuclear cardiology. *J. Nucl. Med.* 46, 1664–1678 (2005).
58. Judenhofer, M.S. *et al.* Simultaneous PET-MRI: a new approach for functional and morphological imaging. *Nat. Med.* 14, 459–465 (2008).
59. Barbour, R. *et al.* MRI-guided optical tomography: prospects and computation for a new imaging method. *IEEE Comput. Sci. Eng.* 2, 63–77 (1995).
60. Ntziachristos, V., Yodh, A.G., Schnall, M. & Chance, B. Concurrent MRI and diffuse optical tomography of breast after indocyanine green enhancement. *Proc. Natl. Acad. Sci. USA* 97, 2767–2772 (2000).

61. Brooksby, B. *et al.* Imaging breast adipose and fibroglandular tissue molecular signatures by using hybrid MRI-guided near-infrared spectral tomography. *Proc. Natl. Acad. Sci. USA* 103, 8828–8833 (2006).
62. Davis, S.C. *et al.* Magnetic resonance-coupled fluorescence tomography scanner for molecular imaging of tissue. *Rev. Sci. Instrum.* 79, 064302 (2008).
63. Fang, Q. *et al.* Combined optical imaging and mammography of the healthy breast: optical contrast derived from breast structure and compression. *IEEE Trans. Med. Imaging* 28, 30–42 (2009).
64. Schulz, R. *et al.* Hybrid system for simultaneous fluorescence and X-ray computed tomography. *IEEE Trans. Med. Imaging* 29, 465–473 (2010).
65. Hyde, D. *et al.* Hybrid FMT-CT imaging of amyloid-beta plaques in a murine Alzheimer's disease model. *Neuroimage* 44, 1304–1311 (2009).
66. Lin, Y., Gao, H., Nalcioglu, O. & Gulsen, G. Fluorescence diffuse optical tomography with functional and anatomical a priori information: feasibility study. *Phys. Med. Biol.* 52, 5569–5585 (2007).
67. Guven, M., Yazici, B., Intes, X. & Chance, B. Diffuse optical tomography with a priori anatomical information. *Phys. Med. Biol.* 50, 2837–2858 (2005).
68. Hintersteiner, M. *et al.* In vivo detection of amyloid-beta deposits by near-infrared imaging using an oxazine-derivative probe. *Nat. Biotechnol.* 23, 577–583 (2005).
69. Cox, B.T., Arridge, S.R., Kostli, K.P. & Beard, P.C. Two-dimensional quantitative photoacoustic image reconstruction of absorption distributions in scattering media by use of a simple iterative method. *Appl. Opt.* 45, 1866–1875 (2006).
70. Rosenthal, A., Razansky, D. & Ntziachristos, V. Fast semi-analytical model-based acoustic inversion for quantitative optoacoustic tomography. *IEEE Trans. Med. Imaging* 29, 1275–1285 (2010).
71. Bowen, T. Radiation-induced thermoacoustic soft-tissue imaging. *Proc. IEEE Ultrason. Symp.* 817–822 (1981).
72. Zemp, R.J. *et al.* Photoacoustic imaging of the microvasculature with a high-frequency ultrasound array transducer. *J. Biomed. Opt.* 12, 010501 (2007).
73. Allen, T.J. & Beard, P.C. Pulsed near-infrared laser diode excitation system for biomedical photoacoustic imaging. *Opt. Lett.* 31, 3462–3464 (2006).
74. Kolkman, R.G.M. *et al.* Photoacoustic determination of blood vessel diameter. *Phys. Med. Biol.* 49, 4745–4756 (2004).
75. Eghtedari, M. *et al.* High sensitivity of in vivo detection of gold nanorods using a laser optoacoustic imaging system. *Nano Lett.* 7, 1914–1918 (2007).
76. Cox, B., Arridge, S. & Beard, P. Estimating chromophore distributions from multiwavelength photoacoustic images. *J. Opt. Soc. Am. A Opt. Image Sci. Vis.* 26, 443–455 (2009).
77. Jetzfellner, T., Rozenthal, A., Englmeier, K., Razansky, D. & Ntziachristos, V. Multispectral optoacoustic tomography by means of normalized spectral ratio. *Opt. Lett.* (in the press).
78. Li, M. *et al.* Simultaneous molecular and hypoxia imaging of brain tumors in vivo using spectroscopic photoacoustic tomography. *Proc. IEEE* 96, 481–489 (2008).
79. Li, L., Zemp, R., Lungu, G., Stoica, G. & Wang, L. Photoacoustic imaging of *lacZ* gene expression in vivo. *J. Biomed. Opt.* 12, 020504 (2007).
80. Kruger, R.A, Kiser, W. Jr., Reinecke, D., Kruger, G. & Miller, K. Thermoacoustic optical molecular imaging of small animals. *Mol. Imaging* 2, 113–123 (2003).
81. Rayavarapu, R. *et al.* Synthesis and bioconjugation of gold nanoparticles as potential molecular probes for light-based imaging techniques. *Int. J. Biomed. Imaging* 2007 29817 (2007).
82. Li, L., Zemp, R.J., Lungu, G., Stoica, G. & Wang, L.V. Photoacoustic imaging of *lacZ* gene expression *in vivo*. *J. Biomed. Opt.* 12, 020504 (2007).
83. Galanzha, E. *et al.* In vivo magnetic enrichment and multiplex photoacoustic detection of circulating tumour cells. *Nat. Nanotechnol.* 4, 855–860 (2009).
84. Vinegoni, C., Pitsouli, C., Razansky, D., Perrimon, N. & Ntziachristos, V. *In vivo* imaging of *Drosophila melanogaster* pupae with mesoscopic fluorescence tomography. *Nat. Methods* 5, 45–47 (2008).
85. Razansky, D. *et al.* Imaging of mesoscopic targets using selective-plane optoacoustic tomography. *Nat. Photonics* 3, 412–417 (2009).Ademonstration of visualizing optical reporter molecules *in vivo* using mesoscopic multispectral optoacoustic tomography.
86. Jain, R.K., Munn, L.L. & Fukumura, D. Dissecting tumour pathophysiology using intravital microscopy. *Nat. Rev. Cancer* 2, 266–276 (2002).Adescription of *in vivo* applications of intravital microscopy in cancer.
87. Wang, T.D., Contag, C.H., Mandella, M.J., Chan, N.Y. & Kino, G.S. Confocal fluorescence microscope with dual-axis architecture and biaxial postobjective scanning. *J. Biomed. Opt.* 9, 735–742 (2004).
88. Sipkins, D.A. *et al.* In vivo imaging of specialized bone marrow endothelial microdomains for tumour engraftment. *Nature* 435, 969–973 (2005).
89. Kleinfeld, D., Mitra, P.P., Helmchen, F. & Denk, W. Fluctuations and stimulus-induced changes in blood flow observed in individual capillaries in layers 2 through 4 of rat neocortex. *Proc. Natl. Acad. Sci. USA* 95, 15741–15746 (1998).
90. Majewska, A.K., Newton, J.R. & Sur, M. Remodeling of synaptic structure in sensory cortical areas in vivo. *J. Neurosci.* 26, 3021–3029 (2006).
91. Germain, R.N. *et al.* An extended vision for dynamic high-resolution intravital immune imaging. *Semin. Immunol.* 17, 431–441 (2005).
92. Molitoris, B.A. & Sandoval, R.M. Intravital multiphoton microscopy of dynamic renal processes. *Am. J. Physiol. Renal Physiol.* 288, F1084–F1089 (2005).
93. Jobsis, F.F. Noninvasive, infrared monitoring of cerebral and myocardial oxygen sufficiency and circulatory parameters. *Science* 198, 1264–1267 (1977).
94. Boas, D.A., Oleary, M.A., Chance, B. & Yodh, A.G. Scattering of diffuse photon fensity eaves ny dpherical inhomogeneities within turbid media—analytic solution and applications. *Proc. Natl. Acad. Sci. USA* 91, 4887–4891 (1994).
95. Schotland, J.C. Continuous-wave diffusion imaging. *J. Opt. Soc. Am. A Opt. Image Sci. Vis.* 14, 275–279 (1997).
96. Cheong, W., Prahl, S. & Welch, A. A review of the optical-properties of biological tissues. *IEEE J. Quantum Electron.* 26, 2166–2185 (1990).
97. Beek, J.F., van Staveren, H.J., Posthumus, P., Sterenborg, H.J.C.M. & van Gemert, M.J.C. The optical properties of lung as a function of respiration. *Phys. Med. Biol.* 42, 2263–2272 (1997).
98. Pogue, B.W. *et al.* Characterization of hemoglobin, water, and NIR scattering in breast tissue: analysis of intersubject variability and menstrual cycle changes. *J. Biomed. Opt.* 9, 541–552 (2004).
99. Niedre, M., Turner, G. & Ntziachristos, V. Time-resolved imaging of optical coefficients through murine chest cavities. *J. Biomed. Opt.* 11, 064017–064011–064017 (2006).